sustainability

MDPI

Article

Enhancing CO_2 Fixation and Wastewater Treatment Performance by Assembling MgFe-LDH on *Chlorella pyrenoidosa*

Huanan Xu [1], Hao Zhou [1], Yinfeng Hua [2], Weihua Chen [3], Jian Wu [3], Zhenwu Long [1], Liang Zhao [1], Lumei Wang [1], Guoqing Shen [1] and Qincheng Chen [1,4,*]

[1] School of Agriculture and Biology, Shanghai Jiao Tong University, 800 Dongchuan Road, Shanghai 200240, China; xuhuanan0409@sjtu.edu.cn (H.X.); dr_zhouhao@sjtu.edu.cn (H.Z.); lzw1020@sjtu.edu.cn (Z.L.); zhaoliang25@sjtu.edu.cn (L.Z.); zjuwlm@163.com (L.W.); gqsh@sjtu.edu.cn (G.S.)
[2] Shanghai Pudong Environmental Protection Energy Development Co., Ltd., Shanghai 200127, China; huayf2015@126.com
[3] Shanghai Liming Resources Reuse Co., Ltd., Shanghai 201209, China; cwh62500@163.com (W.C.); woojan@aliyun.com (J.W.)
[4] Shanghai Yangtze River Delta Eco-Environmental Change and Management Observation and Research Station (Shanghai Urban Ecosystem Research Station), Ministry of Science and Technology, National Forestry and Grassland Administration, 800 Dongchuan Road, Shanghai 200240, China
* Correspondence: chenqincheng@sjtu.edu.cn

Abstract

Microalgae are considered to be a dual solution for CO_2 fixation and biogas slurry purification due to their high photosynthetic efficiency and strong environmental adaptability. However, their application is constrained by the low solubility of CO_2 in the solution environment, which restricts microalgal growth, resulting in low biomass production and poor slurry purification efficiency. In this study, we developed MgFe layered double hydroxide (LDH) that spontaneously combined with *Chlorella pyrenoidosa* to help it concentrate CO_2, thereby increasing biomass yield and purification capacity for food waste biogas slurry. The prepared MgFe-LDH exhibited a typical layered structure with a CO_2 adsorption capacity of 4.44 mmol/g. MgFe-LDH and *C. pyrenoidosa* carried opposite charges, enabling successful self-assembly via electrostatic interaction. Compared with the control, the addition of 200 ppm MgFe-LDH increased *C. pyrenoidosa* biomass and pigment content by 36.82% and 63.05%, respectively. The removal efficiencies of total nitrogen, total phosphorus, and ammonia nitrogen in the slurry were enhanced by 20.04%, 31.54% and 14.57%, respectively. The addition of LDH effectively alleviated oxidative stress in *C. pyrenoidosa* and stimulated the secretion of extracellular polymeric substances, thereby enhancing the stress resistance and pollutant adsorption capabilities. These findings provided a new strategy for the industrial application of microalgal technology in CO_2 fixation and wastewater treatment.

Keywords: layered double hydroxide; microalgae; CO_2 fixation; biogas slurry

check for updates

Academic Editor: Antonio Zuorro

Received: 28 August 2025
Revised: 2 October 2025
Accepted: 6 October 2025
Published: 10 October 2025

Citation: Xu, H.; Zhou, H.; Hua, Y.; Chen, W.; Wu, J.; Long, Z.; Zhao, L.; Wang, L.; Shen, G.; Chen, Q. Enhancing CO_2 Fixation and Wastewater Treatment Performance by Assembling MgFe-LDH on *Chlorella pyrenoidosa*. *Sustainability* **2025**, *17*, 8970. https://doi.org/10.3390/su17208970

Copyright: © 2025 by the authors. Licensee MDPI, Basel, Switzerland. This article is an open access article distributed under the terms and conditions of the Creative Commons Attribution (CC BY) license (https://creativecommons.org/licenses/by/4.0/).

1. Introduction

Under the urgent global demand for CO_2 reduction and biogas slurry treatment, microalgae are regarded as a dual solution [1] to achieve CO_2 fixation [2,3] and biogas slurry purification [4]. This is attributed to their high photosynthetic efficiency, strong environmental adaptability, and capacity to utilize nutrients in biogas slurry. Microalgae can effectively fix CO_2 through photosynthesis while synthesizing biomass [5]. Their carbon fixation efficiency is approximately 10–50 times higher than that of terrestrial plants [6], with the production of 1 kg of microalgae biomass resulting in the fixation of about 1.8 kg of CO_2 [7].

Moreover, microalgae have demonstrated significant potential in the bioremediation of nutrients, emerging contaminants, heavy metals, and pathogens in wastewater [8]. Tan et al. reported that under conditions of CO_2 aeration and high-light intensity (600 μmol/m^2/s), five green microalgae cultures achieved nutrient removal rates within the ranges of 29–81% for NH_4^+-N, 28–66% for TN, and 44–81% for TP when cultivated in diluted swine manure biogas slurry [9]. Wang et al. demonstrated that effective nutrient removal from dairy manure wastewater by *Chlorella* sp. under photoautotrophic conditions, achieving removal rates of 69–80% for COD, 68–89% for NH_4^+-N, and 52–66% for TP [10]. By removing nitrogen and phosphorus components, they help mitigate the risk of eutrophication [11]. Additionally, cultivating microalgae in biogas slurry offers a way to reduce production costs. The effectiveness of microalgae in carbon sequestration and biogas slurry purification is closely related to biomass production during cultivation [12,13]. However, a major practical challenge is the low solubility of CO_2 in solution, which leads to insufficient supply of extracellular inorganic carbon [14,15]. To compensate for this deficiency, microalgae are forced to activate the energy consuming carbon concentration mechanism (CCM) [16,17]. This mechanism actively transports HCO_3^- and upregulates the expression of carbonic anhydrase (CA) and Rubisco enzymes. CCM can locally increase CO_2 concentration but consume additional photosynthetic ATP, thereby constraining growth potential and reducing the carbon fixation rate per unit biomass [18]. Ultimately, microalgae productivity is limited and wastewater purification performance is compromised. Therefore, enhancing CO_2 utilization efficiency is essential to fully utilize the CO_2 fixation and purification capabilities of microalgae and to achieve their large-scale engineering applications.

To address this challenge, researchers have proposed various strategies to enhance microalgal CO_2 fixation efficiency. Genetic engineering of the Calvin cycle is an advanced strategy for enhancing carbon fixation efficiency in microalgae, primarily achieved through optimizing key enzyme activities and redesigning carbon metabolic networks [19,20]. However, this strategy still faces challenges including high metabolic complexity, imprecise regulation of gene expression, and potential ecological risks. Another strategy is to increase the CO_2 supply level in gas–liquid reactors, which directly elevates the concentration of dissolved inorganic carbon in the microalgal culture medium and alleviates carbon insufficiency. Nevertheless, this method often leads to higher energy consumption during production [21,22]. In contrast, co-culturing microalgae with functional materials capable of CO_2 adsorption has attracted growing interest due to its operational simplicity, controllable risks, and absence of additional energy requirements [23]. For example, Allana et al. added and renewed polymeric nanofibers in cultures of *Chlorella fusca* LEB 111 to maximize gas adsorption and desorption potential, resulting in a 21.6% higher biomass concentration and a 23% higher CO_2 biofixation rate compared to the control [24]. Yang et al. introduced Zn/Fe-based metal–organic frameworks nanoparticles into microalgal solutions to overcome low CO_2 solubility, achieving a high CO_2 fixation efficiency of 21.6% and promoting the biomass productivity of 0.240 g/L·d [25]. Tanakit et al. developed living microalgae–loofah biocomposites with immobilized *Scenedesmus acuminatus* TISTR 8457 for highly efficient CO_2 capture from CO_2-rich triethanolamine solution. The biocomposite achieved CO_2 removal rates 3 to 5 times higher than those of the suspended cell system, with the highest removal efficiency reaching 4.34 ± 0.20 $g_{CO_2}/g_{biomass}$ [26]. Furthermore, the co-culture of functional materials with microalgae to enhance wastewater treatment has also been reported. For instance, Qiu et al. demonstrated that nanoscale zerovalent iron not only promoted microalgal biomass accumulation but also alleviated cellular oxidative stress, thereby significantly improving the removal rates of ammonium and phosphate from wastewater [27]. Rehman et al. integrated *Chlorella vulgaris* with algal-biochar, which enhanced the bioremediation process through combined biosorption and biodegradation,

leading to effective phosphate removal from textile wastewater [28]. However, most existing studies focus on utilizing materials to enhance a single function. Co-culture systems that synergistically enhance both CO_2 fixation and wastewater treatment remain scarcely reported. Moreover, the relatively complex synthesis processes and high costs of these materials limit their application in large-scale microalgal industries. Therefore, there is an urgent need to develop novel materials that are cost-effective and capable of enhancing CO_2 fixation efficiency while promoting microalgal growth and proliferation.

Layered double hydroxides (LDHs), due to their low-cost raw materials, easy availability, and straightforward synthesis methods, are considered ideal candidates for large-scale systems among various adsorption materials [29–31]. LDHs possess a 3R-type layered stacking structure, high specific surface area, and abundant surface alkaline sites, which collectively contribute to their efficient and selective adsorption of CO_2 molecules [32–34]. The application of LDH and LDH-derived materials for CO_2 capture has also been widely investigated [35–37]. Aamir et al. developed an exfoliated Ni-Al LDH material with a high specific surface area (210.2 m^2/g) and nanoflower-like structure, which exhibits a CO_2 capture capacity of 0.66 mmol/g [38]. Ayat et al. utilized microwave-assisted homogeneous precipitation via urea hydrolysis to synthesize Mg-Al and Zn-Al LDHs for selective CO_2 capture from methane streams, achieving maximum CO_2 adsorption capacities of 3.25 mmol/g for Mg–Al LDH and 2.47 mmol/g for Zn–Al LDH at 30 °C [39]. LDH are capable of capturing CO_2 in the presence of moisture, making them suitable for application in microalgae cultivation systems [40]. Moreover, LDHs exhibit excellent biocompatibility and have been widely utilized in various fields such as drug delivery, tissue engineering, and ecological restoration [41–43], which provides a reliable safety foundation for their integration with microalgae in co-culture systems. However, their application in the field of microalgae cultivation has not yet been reported.

In this study, we successfully synthesized MgFe-LDH with selective CO_2 adsorption capability. When co-cultured with *Chlorella pyrenoidosa*, the MgFe-LDH underwent self-assembly with the microalgae and functioned as a CO_2 concentrator, thereby significantly improving the algal capacity for CO_2 capture and assimilation. This process resulted in enhanced carbon fixation and biomass accumulation, ultimately improving the ability of *C. pyrenoidosa* to purify biogas slurry. This study aimed to deepen the understanding of the role played by functional materials in improving microalgae cultivation and to provide a feasible strategy for more efficient application of microalgae in CO_2 fixation and biogas slurry purification.

2. Materials and Methods

2.1. Preparation and Characterization of MgFe-LDH

$MgCl_2$ and $FeCl_3$ were dissolved in deionized water at a molar ratio of Mg:Fe = 3:1 to prepare a mixed solution containing 0.3 mol/L $MgCl_2$ and 0.1 mol/L $FeCl_3$. A 3:1 Mg/Fe ratio was selected for the synthesis of MgFe-LDH to favor the formation of LDHs phase with optimal crystallinity and stability LDHs in this study [44,45]. The solution was sonicated for 5 min to ensure uniform mixing and then stirred magnetically for 30 min. While stirring, 1 mol/L NaOH was added dropwise to adjust the pH to 10. After centrifugation, the supernatant was removed, and the precipitate was washed three times with deionized water and freeze-dried to obtain MgFe-LDH. The crystal structure of MgFe-LDH was characterized by X-ray diffraction (XRD) using an X-ray diffractometer (XRD-6100, Shimadzu, Japan), and the data were processed using Jade 6.5 software. The specific surface area was determined by an Autosorb-iQ3 automated specific surface area and porosity analyzer using the Brunauer–Emmett–Teller (BET) method. The CO_2 adsorption performance was measured using an ASAP2020 physical adsorption analyzer (Micromeritics, Norcross, GA,

USA). Prior to measurement, the MgFe-LDH powder was degassed at 120 °C under high vacuum for 2 h. The CO_2 adsorption–desorption isotherms were then measured at 298 K.

2.2. Algal Strain Source and Co-Culture of MgFe-LDH and C. pyrenoidosa

Chlorella pyrenoidosa (FACHB-9) was acquired from the Freshwater Algae Culture Collection at the Institute of Hydrobiology. The pre-culture was carried out in BG11 medium amended with 50 mg/L kanamycin sulfate and constant illumination until the logarithmic growth phase was reached. To reduce potential particle aggregation or shading effects [46,47], the culture system was maintained under continuous aeration. The initial concentration of *C. pyrenoidosa* was ≤0.1 g/L. A 200 mL culture system was set up in a 250 mL conical flask. The growth of *C. pyrenoidosa* was assessed by cell density and dry weight. Cell density was determined using a hemocytometer under a microscope. For dry weight measurement, the collected algal suspension was centrifuged at 5000 rpm for 5 min, washed with deionized water, and dried at 80 °C until constant weight was achieved. The growth rate (P, $\times 10^6$ cell/(mL·d)) was calculated as follows:

$$P = \frac{X_1 - X_0}{t_1 - t_0} \quad (1)$$

where X_0 and X_1 ($\times 10^6$ cell/mL) represent the biomass concentrations at time points t_0 (d) and t_1 (d), respectively.

For the co-culture system, MgFe-LDH was initially dispersed in the culture medium and sonicated to achieve a homogeneous suspension, ensuring uniform particle distribution prior to the inoculation of *C. pyrenoidosa.* The experimental groups were designated as MgFe-LDH$_x$, where x indicates the dosage (ppm) of MgFe-LDH added to the co-culture system. When necessary, the pH of the suspension was adjusted with 0.1 mol/L NaOH or 0.1 mol/L HCl before use. To observe the microstructure of the co-culture system, the algal suspension was harvested on day 4, centrifuged at 2000 rpm for 10 min, and the precipitate was fixed overnight in a mixture containing 2.5% glutaraldehyde and 2% paraformaldehyde. The fixed sample was then imaged using scanning electron microscopy (SEM5000X, Ciamite, Hefei, China).

2.3. Measurement of Pigment Content

Pigments were extracted from *C. pyrenoidosa* using methanol. 5 mL of algal suspension were centrifuged at 8000 rpm for 5 min, and the supernatant was discarded. Subsequently, 5 mL of methanol were added to the pellet, and the mixture was agitated on a shaker for 10 min, followed by dark extraction for 20 min. The mixture was then centrifuged again at 8000 rpm for 5 min. The absorbance of the supernatant was measured at 470 nm, 666 nm, and 653 nm using a spectrophotometer to calculate the pigment content of *C. pyrenoidosa.*

2.4. Intracellular Oxidative Stress Activity in C. pyrenoidosa

The level of reactive oxygen species (ROS) was measured using a kit from Fuzhou Feijin Biotechnology Co., Ltd. (Fuzhou, China). The fluorescent probe H_2DCFDA is hydrolyzed by intracellular esterases to generate DCFH, which is then oxidized by intracellular ROS to produce fluorescent DCF. The fluorescence intensity was measured using a SpectraMax i3x (Molecular Devices, LLC., San Jose, CA, USA) microplate reader at an excitation wavelength (Ex) of 488 nm and an emission wavelength (Em) of 525 nm. The initial ROS level of pure *C. pyrenoidosa* was set to 1.

The harvested algal suspension was centrifuged at 5000 rpm for 15 min at 4 °C and resuspended in 0.05 M phosphate-buffer solution (PBS, pH 7.8). The sample was sonicated for 30 min on ice and then centrifuged at 10,000 rpm for 10 min at 4 °C. The supernatant

was discarded, and the pellet was resuspended in 1 mL of PBS (pH 7.0). After grinding in liquid nitrogen, the sample was reconstituted in PBS to a final volume of 3.0 mL and centrifuged again under the same conditions. the supernatant was collected as the enzyme extract for the determination of malondialdehyde (MDA) and superoxide dismutase (SOD). MDA content was measured using the thiobarbituric acid method. SOD activity was assessed using the photoreduction method with nitroblue tetrazolium, which measures the inhibition of superoxide-dependent reduction.

2.5. Extraction and Three-Dimensional Fluorescence Analysis of Extracellular Polymeric Substances (EPS)

The harvested biogas slurry was centrifuged at 5000 rpm for 10 min at 4 °C and filtered through a 0.45 μm filter membrane to remove cell debris. The EPS was analyzed using a PerkinElmer fluorescence spectrometer (FL6500, PerkinElmer, Waltham, MA, USA). Three-dimensional excitation-emission matrix (3D-EEM) fluorescence spectra were acquired with Ex ranging from 220 to 450 nm, and Em ranging from 250 to 600 nm, with a scanning interval of 5 nm for both.

2.6. Analysis of Biogas Slurry Water Quality Indicators

The biogas slurry was collected from the anaerobic membrane effluent at Shanghai Pudong Environmental Protection Energy Development Co., Ltd. (Shanghai, China). Its initial composition is provided in Table S1. The culture medium was sampled on days 0, 2, 4, 6, and 8 of algal cultivation, filtered through a 0.45 μm filter membrane, and used to test the changes in biogas slurry water quality indicators. The indicators were measured against pure water as a control using a Hach DRB200 digestion instrument to digest the samples, and a Hach DR500 spectrophotometer to measure the absorbance of total nitrogen (TN), total phosphorus (TP), and ammonia nitrogen (NH_3-N) samples. For TN, 4 mL of sample was mixed with 2 mL of alkaline persulfate solution, digested at 120 °C for 30 min, then cooled and adjusted with 0.5 mL of HCl and 3.5 mL of pure water before measuring absorbance at 220 nm and 275 nm. For TP, 5 mL of sample was combined with 1 mL of persulfate solution, digested at 120 °C for 30 min, then cooled and treated with 3 mL of pure water, 0.2 mL of ascorbic acid, and 0.5 mL of molybdate solution before measuring absorbance at 700 nm after 15 min. For NH3-N, 10 mL of sample was mixed with 0.2 mL of potassium sodium tartrate solution and 0.2 mL of Nessler's reagent, then measured at 420 nm after 10 min. For Chemical Oxygen Demand (COD), 2 mL of sample was treated with 0.08 g of mercuric sulfate and 3 mL of digestion solution, digested at 150 °C for two hours, and measured using a Hach DR1010 COD tester (Hach, Loveland, CO, USA).

3. Results and Discussion

3.1. Self-Assembly of MgFe-LDH and C. pyrenoidosa

MgFe-LDH was successfully synthesized via co-precipitation. The XRD patterns in Figure 1a confirmed the structural characteristics of the prepared MgFe-LDH, matching the standard card of hydrotalcite (PDF#89-0460) with distinct diffraction peaks corresponding to the (003), (006), (009), and (110) crystal planes. The slight leftward shift in the diffraction peaks might be attributed to the substitution of Fe in MgFe-LDH for Al in the reference MgAl-LDH. These characteristic peaks indicated that the synthesized material has high crystallinity and a well-ordered layered structure. The average particle size of MgFe-LDH was 4197.42 nm (Figure S1), with a specific surface area of 27.806 m^2/g. Notably, it exhibited a CO_2 adsorption capacity of 4.44 mmol/g (Figure 1b).

The surface charge of MgFe-LDH and *C. pyrenoidosa* is crucial for self-assembly. Figure 1c illustrated the changes in zeta potential of both under different pH conditions.

The zeta potential of MgFe-LDH remained positive across a pH range of 4 to 10, although it decreased from 23.93 mV to 9.66 mV. As is well known, the cell wall of microalgae is composed of microfibrils formed by polysaccharides and proteins, carrying a negative charge. In this study, the zeta potential of *C. pyrenoidosa* ranged from −12.72 mV to −20.49 mV in the pH range of 4 to 10. Therefore, the opposite charges on the surfaces of MgFe-LDH and *C. pyrenoidosa* facilitated their self-assembly via electrostatic attraction. As illustrated in Figure 1d, the formation of the MgFe-LDH/*C. pyrenoidosa* hybrid could be directly observed under a 400× microscope. SEM images in Figure 1e revealed more details of the self-assembly system. The spherical *C. pyrenoidosa* and the irregular flake-like LDH spontaneously combined in the solution. It's noted that flocculent EPS were observed deposited at the interfaces between *C. pyrenoidosa* and MgFe-LDH, suggesting that EPS also played a significant role in bridging and stabilizing the assembly. This self-assembly structure was anticipated to enhance the local concentration of CO_2 by MgFe-LDH near the microalgae, thereby potentially alleviating carbon limitation for algal growth.

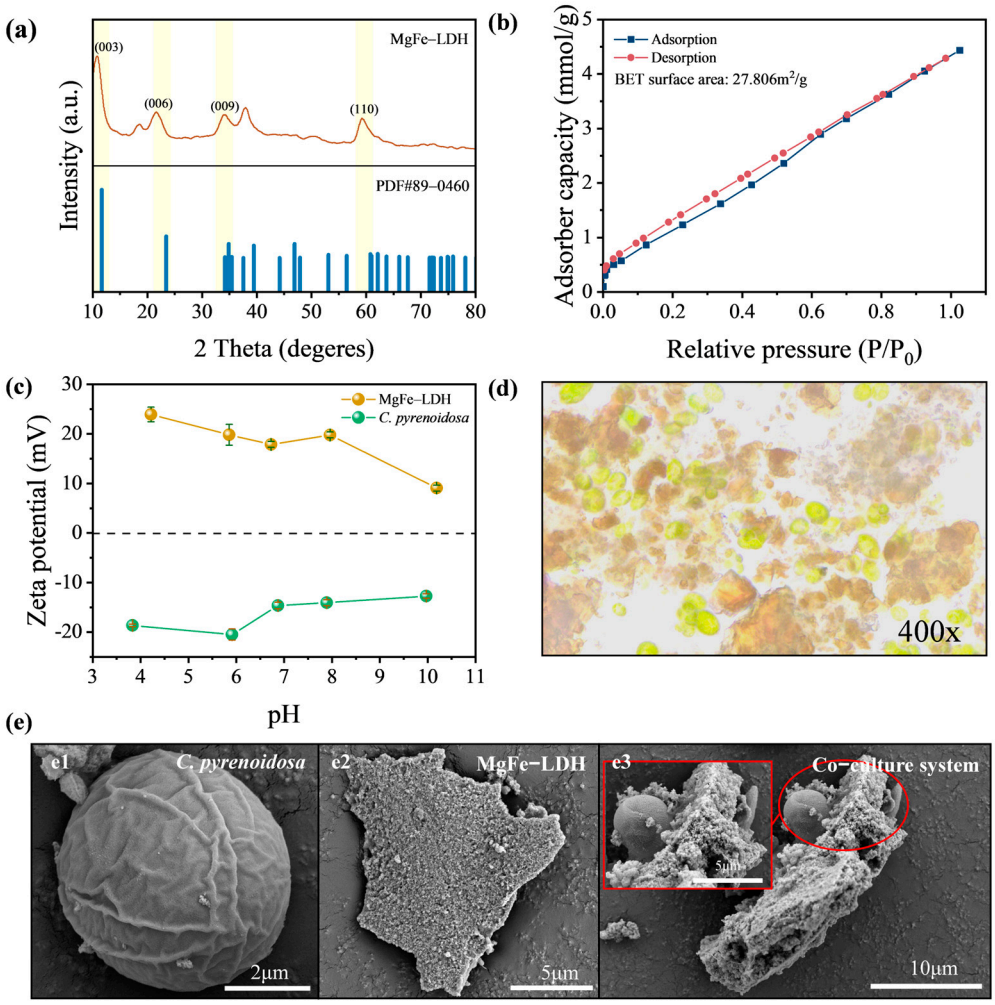


Figure 1. Self-assembly of MgFe-LDH and *C. pyrenoidosa*. (**a**) XRD pattern of MgFe-LDH; (**b**) CO_2 adsorption capacity of MgFe-LDH; (**c**) zeta potential of MgFe-LDH and *C. pyrenoidosa*; (**d**) microscopic image of MgFe-LDH/*C. pyrenoidosa* co-culture system at 400×; (**e**) SEM images of *C. pyrenoidosa*, MgFe-LDH and MgFe-LDH/*C. pyrenoidosa* co-culture system.

3.2. The Effect of MgFe-LDH on the Growth and CO_2 Fixation of C. pyrenoidosa

The effect of MgFe-LDH on the growth of *C. pyrenoidosa* was investigated, with dry weight used to assess the carbon fixation performance of *C. pyrenoidosa.* Figure 2a showed the growth curves of *C. pyrenoidosa* under different MgFe-LDH dosages over a 4-day

cultivation period, and Figure 2b illustrated the changes in growth rate. The maximum cell density in the control group reached 4.22×10^6 cell/mL, with a peak growth rate of 1.09×10^6 cell/(mL·d) on the third day. When MgFe-LDH was added at concentrations of ≥100 ppm, the cell density and growth rate of *C. pyrenoidosa* exceeded those of the control, indicating a promotive effect on *C. pyrenoidosa* growth. Specifically, with 200 ppm MgFe-LDH addition, the cell density reached the maximum value of 9.34×10^6 cell/mL, and the growth rate increased to the highest value of 25.37×10^6 cell/(mL·d). However, higher dosages of MgFe-LDH dosage led to noticeable adsorption and sedimentation of *C. pyrenoidosa* cells in the early stages of cultivation. Although the cell density at harvest for the 100 ppm treatment (7.22×10^6 cell/mL) was lower than that for the 200 ppm MgFe-LDH treatment, both 100 ppm and 200 ppm MgFe-LDH additions showed comparable growth-promoting effects on *C. pyrenoidosa* growth during the first three days of cultivation. Based on their significant efficacy in promoting algal growth, evidenced by the highest cell density and peak growth rate, MgFe-LDH concentrations of 100 and 200 ppm were selected as the optimal dosages for further investigation. As shown in Figure 2c,d, the dry weight and pigment content of each treatment were measured on day 4. Consistent with the cell density results, the dry weight of *C. pyrenoidosa* in the 100 ppm and 200 ppm self-assembly systems increased by 25.00% and 36.82%, respectively, compared to the control. Similarly, the pigment content increased by 29.78% and 63.05%, suggesting that MgFe-LDH not only promoted biomass accumulation but also enhanced the photosynthetic capacity of *C. pyrenoidosa.*

Both Mg and Fe elements are beneficial to photosynthesis and biomass accumulation [48–51]. To exclude the potential influence of ions dissolved from MgFe-LDH in the solution, we tested the chemical stability of MgFe-LDH in the culture medium. The leachate after centrifuging MgFe-LDH suspensions was collected to culture *C. pyrenoidosa.* As indicated in Figure 2e, the Mg and Fe concentrations in the leachate were 25.22 mg/L and 0.090 mg/L for the 100 ppm treatment, and 15.40 mg/L and 0.05 mg/L for the 200 ppm treatment, respectively. Figure 2f showed the cell density of *C. pyrenoidosa* cultured in the leachate for 4 days. The cell densities for MgFe-LDH_{100} and MgFe-LDH_{200} were 5.47×10^6 cell/mL and 8.13×10^6 cell/mL, respectively, both of which were lower than that of the control (15.30×10^6 cell/mL). These results demonstrated that the dissolved Mg and Fe ions in the solution did not promote the growth of *C. pyrenoidosa*, confirming that the observed promotive effects were primarily due to the direct interaction between the MgFe-LDH and microalgae.

CO_2 is typically supplied to microalgal culture media in the form of bubbles, forming four main inorganic carbon species (CO_2, H_2CO_3, HCO_3^-, CO_3^{2-}) [25]. The pH of the medium plays a critical role in determining the dominant carbon species [52–54], which may subsequently influence the ability of LDH materials to enhance microalgal CO_2 fixation. Therefore, *C. pyrenoidosa* was cultivated under different initial pH conditions to evaluate whether MgFe-LDH promoted microalgal growth by increasing local CO_2 concentration. For consistency and clearer comparison, an MgFe-LDH concentration of 200 ppm was used throughout these experiments. As shown in Figure 3a,b, the cell density and medium pH were monitored under various initial pH conditions. The results indicated that compared with the control, the cell density of *C. pyrenoidosa* in the co-culture group was significantly increased by 26.15%, 10.76%, and 6.23% for initial pH values of 6, 7, and 8, respectively. The stronger promoting effect observed at lower pH may be attributed to the higher solubility of CO_2 under acidic conditions, which allowed MgFe-LDH to function more effectively as a CO_2 concentrator. Additionally, an experiment with 2% CO_2 injection was conducted to examine the effect of MgFe-LDH on C. pyrenoidosa growth under high CO_2 concentration conditions. As shown in Figure S2, the pH values measured on day 1 and day 4 after

the injection of 2% CO_2 indicated that CO_2 supplementation effectively stabilized the pH variation in the culture system. As illustrated in Figure 3c, the cell density in the control group reached 74.87 × 10^6 cells/mL, while the values for the 100 ppm and 200 ppm MgFe-LDH treatments were 72.89 × 10^6 cells/mL and 73.78 × 10^6 cells/mL, respectively. No significant differences were observed among the three groups, suggesting that the presence of abundant dissolved CO_2 diminished the relative contribution of MgFe-LDH to carbon availability.

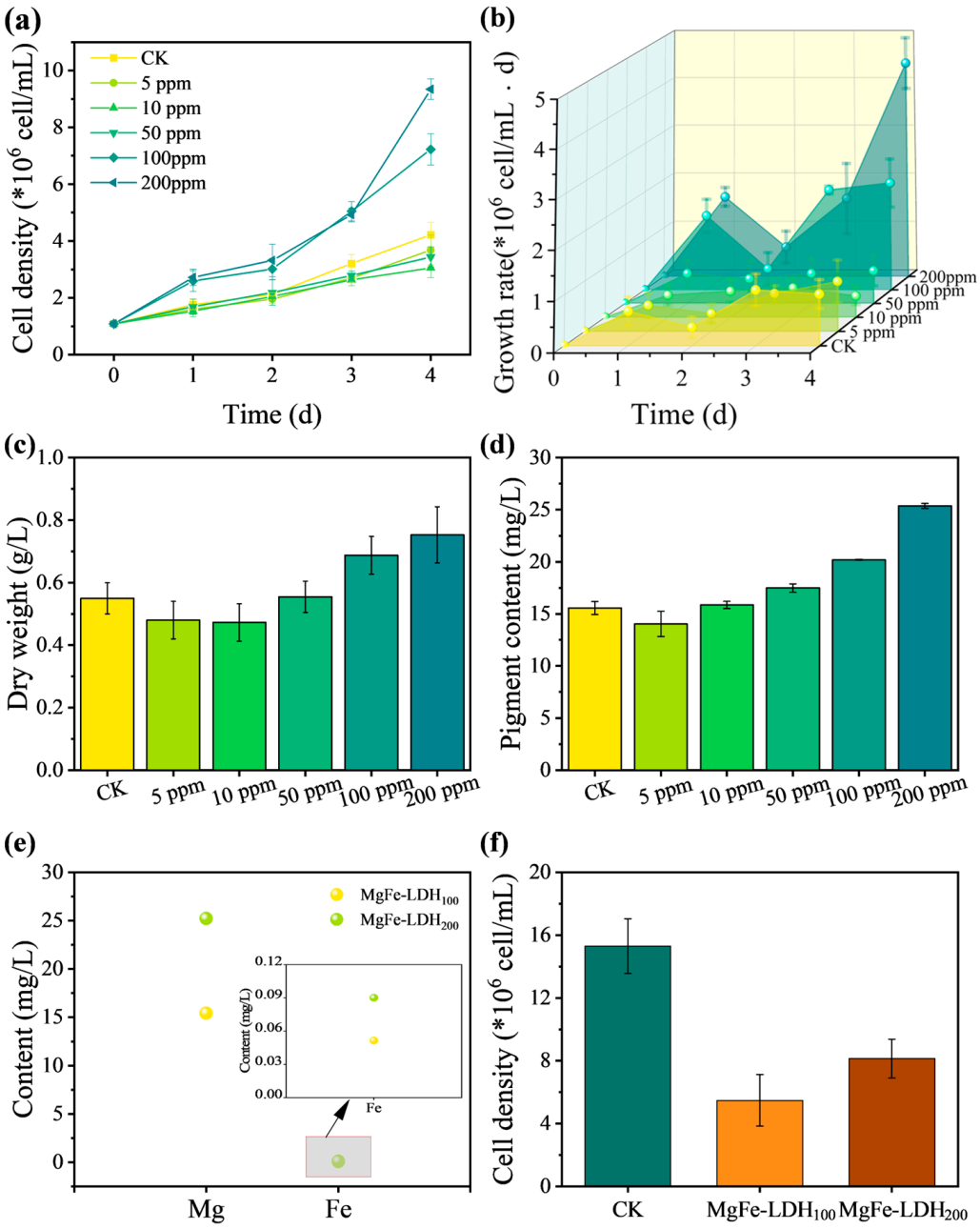


Figure 2. The effect of MgFe-LDH on *C. pyrenoidosa* growth. (**a**) Growth curve of *C. pyrenoidosa*; (**b**) growth rate curve of *C. pyrenoidosa*; (**c**) biomass accumulation of *C. pyrenoidosa* under different treatments on day 4; (**d**) pigment content of *C. pyrenoidosa* under different treatments on day 4; (**e**) concentrations of Mg and Fe elements in the leachate; (**f**) cell density of *C. pyrenoidosa* after 4 days of cultivation in the leachate.

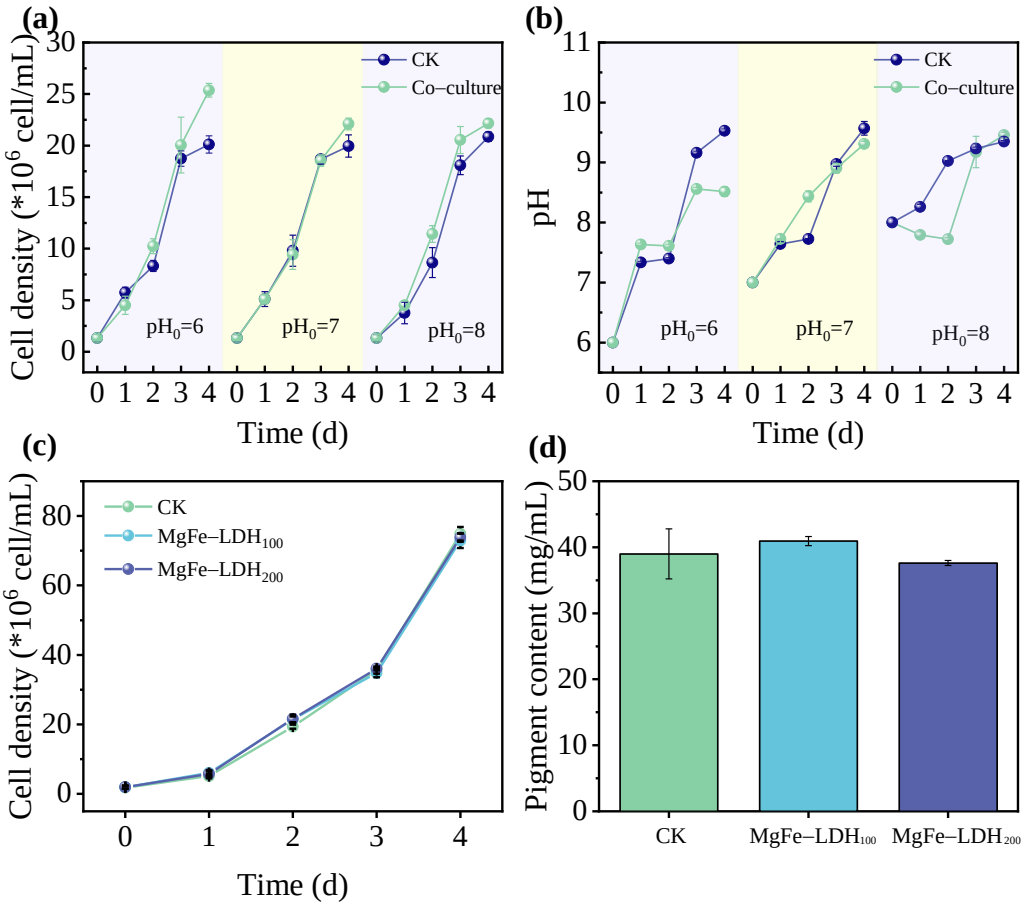


Figure 3. Validation of the MgFe-LDH effect on CO_2 fixation by *C. pyrenoidosa*. (**a**) Cell density of *C. pyrenoidosa* under different initial pH conditions (pH_0 = 6, 7, and 8); (**b**) culture medium pH changes in 4 days; (**c**) cell density of *C. pyrenoidosa* under high CO_2 concentration conditions (2% CO_2); (**d**) pigment content of *C. pyrenoidosa* under high CO_2 concentration conditions (2% CO_2). Data represent mean ± SD (n = 3).

3.3. Enhancement of Biogas Slurry Purification by C. pyrenoidosa with MgFe-LDH and the Underlying Mechanism

To evaluate the effect of MgFe-LDH addition on the purification of biogas slurry by *C. pyrenoidosa*, the biogas slurry was diluted by a factor of two and used as the culture medium to cultivate *C. pyrenoidosa* in 250-mL conical flasks over an 8-day period. The components of the biogas slurry after dilution are shown in Table S1. As shown in Figure 4a, the dry weight of *C. pyrenoidosa* was 0.77 g/L for the control, 1.09 g/L for the MgFe-LDH_{100} treatment, and 1.52 g/L for the MgFe-LDH_{200} treatment. These results indicated that the addition of MgFe-LDH significantly promoted the biomass accumulation of *C. pyrenoidosa* in the biogas slurry, and this effect was positively correlated with the amount of MgFe-LDH added. A similar trend was observed in pigment content (Figure 4b), further confirming the growth-promoting effect of MgFe-LDH.

Figure 4c–f show the removal rates of TN, TP, NH_3-N, and COD from the biogas slurry by *C. pyrenoidosa* after the addition of MgFe-LDH. After 8 days of cultivation, the MgFe-LDH_{100} and the MgFe-LDH_{200} treatment removed 93.67% and 96.86% of TN, respectively, both significantly higher than the control's 78.03%. Similarly, TP removal rate reached 69.80% and 73.40% in the MgFe-LDH-treated groups, compared to 55.80% in the control. NH_3-N removal rate was also improved, with rates of 84.67% and 88.94% in the MgFe-LDH_{100} and MgFe-LDH_{200} treatments, respectively, versus 77.63% in the control. Although MgFe-LDH enhanced COD removal rate in the early stages, no significant differences were

observed among the treatments by day 8, with final removal rates of 86.77%, 88.78%, and 90.67% for the control, MgFe-LDH$_{100}$, and MgFe-LDH$_{200}$ groups, respectively. In summary, the addition of MgFe-LDH significantly improved the carbon fixation capacity, growth, and nutrient removal efficiency of *C. pyrenoidosa* cultivated in biogas slurry. The enhanced biogas slurry purification capability of *C. pyrenoidosa* with MgFe-LDH addition was not only due to the promotion of carbon fixation but was also closely related to the increased stress resistance of *C. pyrenoidosa*.

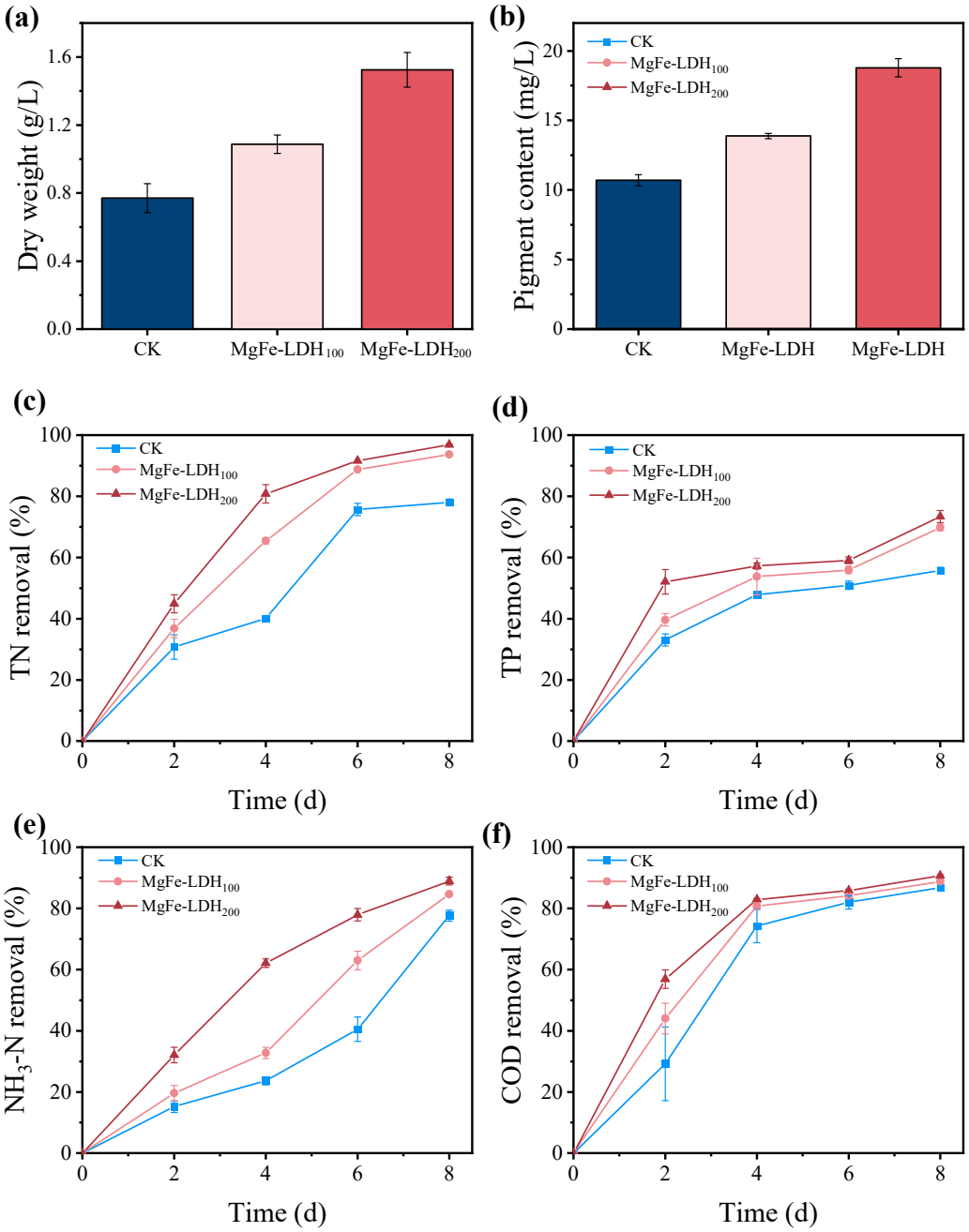


Figure 4. Effect of MgFe-LDH on nutrient removal by *C. pyrenoidosa*; (**a**) dry weight of *C. pyrenoidosa*; (**b**) pigment content of *C. pyrenoidosa*; (**c**) TN removal; (**d**) TP removal rate; (**e**) NH_3-N removal; (**f**) COD removal.

Figure 5 presented the antioxidant capacity of *C. pyrenoidosa* under different treatments, including the ROS level, SOD activity, and MDA content. Over the cultivation period, the relative ROS levels in the treatments with added MgFe-LDH increased from 145.07% to

229.60% in 100 ppm group and increased from 165.85% to 262.36% in 200 ppm group. This increase may be due to the stress response to pollutants in the biogas slurry. The relative ROS level of the control group exhibited minimal change, from 204.24% on the first day to 192.85% on the eighth day, but remained at a relatively high level. Notably, during the early cultivation stage, ROS levels in both MgFe-LDH treatments were lower than in the control, suggesting that MgFe-LDH initially alleviated oxidative stress. This protective effect may be attributed to the adsorptive capacity of LDH, which could reduce the concentration of toxic compounds in the immediate microenvironment of the algal cells. Figure 5b showed the changes in SOD activity. SOD is an important antioxidant enzyme in plants that can catalyze the dismutation of superoxide anions into oxygen and hydrogen peroxide. Compared with the control, the SOD activity in the MgFe-LDH treatments significantly increased on the eighth day. The 100 ppm treatment reached 81.42 U/mgprot and the 200 ppm treatment reached 93.32 U/mgprot, both higher than 71.53 U/mgprot of the control. This indicated that MgFe-LDH can strengthen the antioxidant defense system of *C. pyrenoidosa*, thereby increasing its tolerance to pollutants in the biogas slurry. Figure 5c showed the changes in MDA content. MDA is a product of lipid peroxidation in membranes, and its increased content is usually associated with cell membrane damage. Figure 5c show that despite higher final ROS levels, MDA content in the MgFe-LDH treatments (2.50 and 2.08 nmol/mgprot) was significantly lower than in the control (9.82 nmol/mgprot). This dissociation between ROS levels and lipid peroxidation further confirms that MgFe-LDH helped maintain membrane integrity, possibly through direct interaction with cell surfaces or by modifying the stressor profile experienced by the microalgae. These findings demonstrated that MgFe-LDH enhanced the algal tolerance to biogas slurry stress through multiple mechanisms. Initially, MgFe-LDH provided direct protection against oxidative stressors, and subsequently induced a more robust antioxidant enzyme response that effectively managed oxidative damage while preserving membrane integrity.

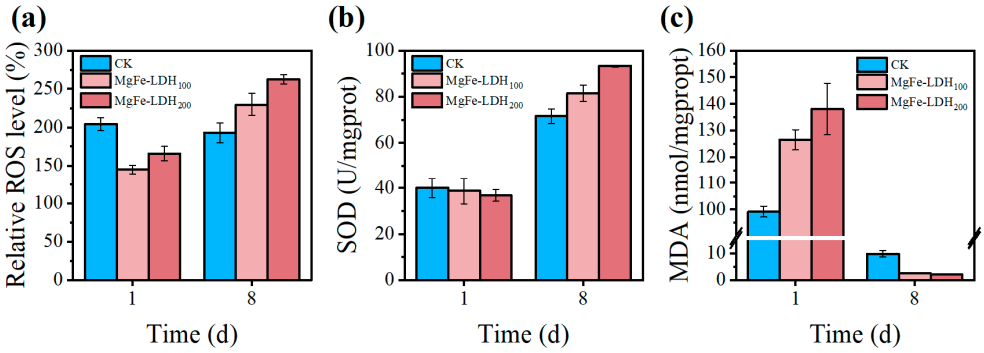


Figure 5. The antioxidant capacity of *C. pyrenoidosa* under different treatments in biogas slurry. (**a**) relative ROS levels of *C. pyrenoidosa* (The initial ROS level of pure *C. pyrenoidosa* was set to 1); (**b**) SOD of *C. pyrenoidosa*; (**c**) MDA of *C. pyrenoidosa*. Data are presented as mean ± SD (n = 3).

The secretion of EPS is related to cell surface adhesion, biofilm formation and pollutant removal [55,56], influencing the performance and stability of the co-culture system. As observed in the SEM images (Figure 1e), the presence of MgFe-LDH stimulated substantial secretion of EPS by *C. pyrenoidosa*. To further evaluate dynamic changes in EPS secretion and composition, 3D fluorescence spectra of EPS were analyzed on the first day and the eighth day (Figure 6). In all treatments, two peaks were identified in the 3D-EMM spectra. Peak A, located in region III, is associated with fulvic acid-like substances, which play crucial roles in nutrient cycling, metal complexation, and the transport of pollutants in the environment [57,58]. Peak B is indicative of humic acid-like substances, another key component of EPS known for its role in adsorbing and binding pollutants [59,60]. When

exposed to biogas slurry after 1 day, a slight increase in the fluorescence intensity of peak A was observed in the system with MgFe-LDH, suggesting that MgFe-LDH promoted the early accumulation of fulvic acid-like components within the EPS. After 8 days of cultivation (Figure 6d–f), the fluorescence intensities of both Peak A and Peak B across all treatments showed a marked increase compared to the first day. This enhancement indicated that *C. pyrenoidosa* continuously secretes EPS as a protective mechanism against environmental stressors present in the biogas slurry. Notably, treatments supplemented with MgFe-LDH exhibited stronger fluorescence intensities for both peaks. This observation implied that the presence of MgFe-LDH appeared to act as an effective promoter of EPS production, enhancing the microalgae's ability to withstand and adapt to the stressful conditions of the biogas slurry. This promoting effect of MgFe-LDH could be attributed to its ability to directly promote EPS production, create a more favorable microenvironment for synthesis, and provide surfaces for EPS to adhere to. By promoting the secretion of EPS, MgFe-LDH could improve the microalgae's capacity to form biofilms, which are known to be more effective in pollutant removal and stress resistance [61]. This discovery highlighted the potential of using MgFe-LDH as a biostimulant to improve the performance of microalgae in wastewater treatment.

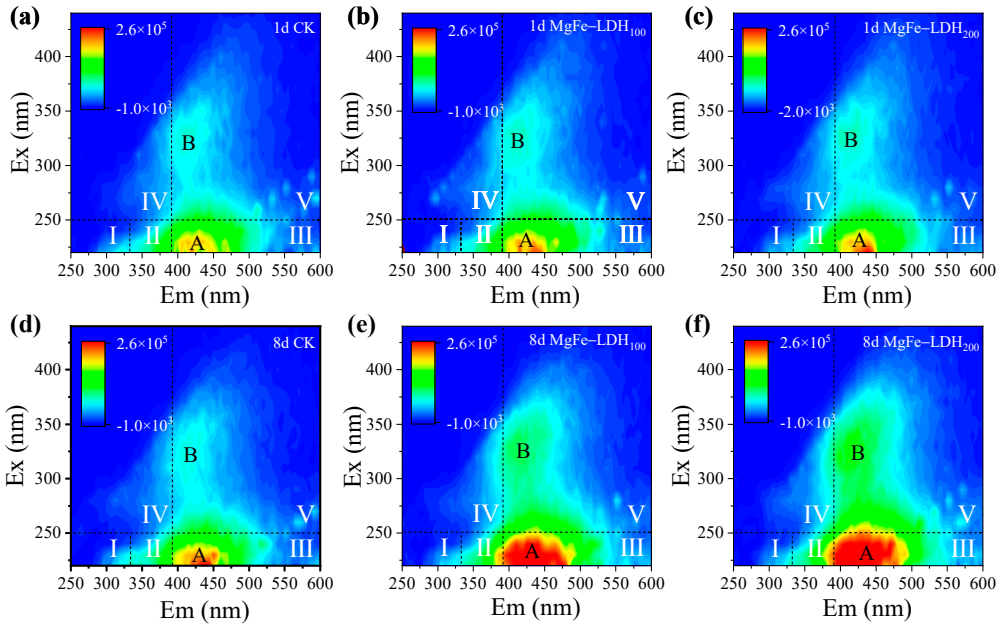


Figure 6. Three-dimensional fluorescence of EPS. (**a**–**c**) 3D fluorescence analysis of EPS of *C. pyrenoidosa* on day 1; (**d**–**f**) 3D fluorescence analysis of EPS of *C. pyrenoidosa* on day 8 (the identified regions correspond to: regions I and II (Ex < 250/Em < 380 nm), aromatic proteins such as complexion, e.g., tyrosine-like substances; region III (Ex < 250/Em > 380 nm), fulvic acid-like; region IV (Ex > 250/Em < 380 nm) microbial metabolic by-products, e.g., tryptophan-like substances; region V (Ex > 280/Em > 380 nm), humic-like organic matter [62]).

4. Conclusions

This study successfully developed a hybrid system based on MgFe-LDH and *C. pyrenoidosa* that synergistically enhanced CO_2 fixation and biogas slurry purification. The synthesized MgFe-LDH exhibited a typical layered structure and a high CO_2 adsorption capacity (4.44 mmol/g). It can spontaneously combine with microalgae through electrostatic interactions, forming a stable self-assembled system without necessitating external energy input. Unlike simply adding adsorbents to the culture, the electrostatic self-assembly creates an intimate association between the microalgae and the LDH, allowing for localized CO_2 enrichment directly at the algal cell surface. This intimate association significantly

improved the CO_2 fixation efficiency of *C. pyrenoidosa*, increasing its biomass and pigment content by 36.82% and 63.05%, respectively. In terms of biogas slurry treatment, the system with MgFe-LDH addition enhanced the removal rates of TN, TP, and NH_3-N by 20.04%, 31.54%, and 14.57%, respectively. The superiority of this self-assembly strategy lies in its dual-action mechanism. MgFe-LDH not only functioned as a CO_2 concentrator to promote carbon assimilation but also improved antioxidant capacity and increased secretion of EPS, which enhanced the stress tolerance and pollutant adsorption ability of the microalgae. The system concurrently achieves dual benefits of effective CO_2 fixation and wastewater purification, thereby offering a more holistic and sustainable solution compared to single-purpose technologies.

Due to its cost-effective synthesis, energy-efficient self-assembly, and dual functionality in CO_2 fixation and wastewater purification, the MgFe-LDH/*C. pyrenoidosa* system exhibits considerable potential for actual applications. However, several limitations must be addressed to ensure the technology's broader applicability and sustainability. As this study was conducted at the laboratory scale, pilot-scale validation is necessary to assess performance under realistic conditions. Additionally, the long-term environmental impacts of LDH accumulation and its ecological consequences also require thorough evaluation. Furthermore, a comprehensive cost–benefit analysis is essential to evaluate the economic feasibility for industrial applications. Future research may focus on optimizing the synthesis process of MgFe-LDH, evaluating environmental safety, and exploring recycling and regeneration strategies. Inspired by the integrated test strategy framework proposed by Strotmann et al. [63], which systematically bridges laboratory discovery to real-world application through tiered assessments, we suggest incorporating a similar multi-stage assessment into future scaling efforts. This approach would facilitate the translation of the MgFe-LDH/*C. pyrenoidosa* system into practical industrial applications.

Supplementary Materials: The following supporting information can be downloaded at https://www.mdpi.com/article/10.3390/su17208970/s1, Figure S1: Size measurements of *C. pyrenoidosa* and MgFe-LDH; Figure S2: pH values on day 1 and day 8 of CK, MgFe-LDH_{100} co-culture system and MgFe-LDH_{200} co-culture system under high CO_2 concentration conditions (2%CO_2); Table S1: The initial composition of biogas slurry.

Author Contributions: Conceptualization, Q.C. and H.X.; methodology, H.X.; validation, H.X.; formal analysis, H.X. and L.Z.; investigation, H.X., Y.H., W.C., J.W. and Z.L.; resources, Y.H., W.C., J.W. and G.S.; data curation, H.X. and H.Z.; writing—original draft preparation, H.X.; writing—review and editing, Q.C., L.W. and G.S.; visualization, H.X. and H.Z.; supervision, Q.C. and G.S.; project administration, H.X. and Q.C.; funding acquisition, Q.C. All authors have read and agreed to the published version of the manuscript.

Funding: This research was funded by the National Natural Science Foundation of China (No. 42207004), and Shanghai Municipal Agricultural Science and Technology Innovation Project (T2024303).

Institutional Review Board Statement: Not applicable.

Informed Consent Statement: Not applicable.

Data Availability Statement: Data is contained within the article.

Conflicts of Interest: Yinfeng Hua is employed by Shanghai Pudong Environmental Protection Energy Development Co., Ltd., and Weihua Chen and Jian Wu are employed by Shanghai Liming Resources Reuse Co., Ltd. The remaining authors declare that the research was conducted in the absence of any commercial or financial relationships that could be construed as a potential conflict of interest.

Abbreviations

The following abbreviations are used in this manuscript:

CCM	Carbon concentration mechanism
CA	Carbonic anhydrase
LDH	Layered double hydroxide
XRD	X-ray diffraction
PBS	phosphate-buffer solution
MDA	Malondialdehyde
SOD	Superoxide dismutase
ROS	Reactive oxygen species
Ex	Excitation wavelength
Em	Emission wavelength
EPS	Extracellular polymeric substances
3D-EEM	Three-dimensional excitation-emission matrix
TN	Total nitrogen
TP	Total phosphorus
NH_3-N	Ammonia nitrogen
COD	Chemical oxygen demand

References

1. Goswami, R.K.; Mehariya, S.; Karthikeyan, O.P.; Gupta, V.K.; Verma, P. Multifaceted Application of Microalgal Biomass Integrated with Carbon Dioxide Reduction and Wastewater Remediation: A Flexible Concept for Sustainable Environment. *J. Clean. Prod.* **2022**, *339*, 130654. [CrossRef]
2. Nguyen, L.N.; Vu, M.T.; Vu, H.P.; Johir, M.A.H.; Labeeuw, L.; Ralph, P.J.; Mahlia, T.M.I.; Pandey, A.; Sirohi, R.; Nghiem, L.D. Microalgae-Based Carbon Capture and Utilization: A Critical Review on Current System Developments and Biomass Utilization. *Crit. Rev. Environ. Sci. Technol.* **2023**, *53*, 216–238. [CrossRef]
3. Ramanna, L.; Ansari, F.A.; Rawat, I.; Bux, F. Microalgae-Driven Carbon Sequestration and Bio-Fertiliser: Steps towards a Sustainable Future. *Chem. Eng. J.* **2025**, *519*, 164892. [CrossRef]
4. Zhang, Y.; Yin, Z.; Xie, J.; Zou, X.; Dai, Y.; He, D.; Li, J. Efficient Treatment of Actual Biogas Slurry by Chlorella Sorokiniana: Nutrient Recovery and Biomass Production. *J. Water Process Eng.* **2024**, *66*, 106007. [CrossRef]
5. Xu, X.; Gu, X.; Wang, Z.; Shatner, W.; Wang, Z. Progress, Challenges and Solutions of Research on Photosynthetic Carbon Sequestration Efficiency of Microalgae. *Renew. Sustain. Energy Rev.* **2019**, *110*, 65–82. [CrossRef]
6. Ma, J.; Cui, Y.; Sun, F.; Zhou, R.; Liu, F.; Cao, K.; Zhu, B.; Zhang, H.; Meng, C.; Chen, G.; et al. Strategies for Enhancing Microalgal Carbon Sequestration: A Review on Strain Development, Culture System Optimization, Parameter Control, and Metabolic Engineering. *Bioresour. Technol.* **2025**, *435*, 132868. [CrossRef]
7. Li, J.; Tang, X.; Pan, K.; Zhu, B.; Li, Y.; Ma, X.; Zhao, Y. The Regulating Mechanisms of CO_2 Fixation and Carbon Allocations of Two *Chlorella* sp. Strains in Response to High CO_2 Levels. *Chemosphere* **2020**, *247*, 125814. [CrossRef]
8. Hou, C.; Zhao, J.; Huang, B.; Zhou, X.; Zhang, Y. Microalgae-Based Technologies for Carbon Neutralization and Pollutant Remediation: A Comprehensive and Systematic Review. *Resour. Conserv. Recycl.* **2024**, *202*, 107323. [CrossRef]
9. Tan, F.; Wang, Z.; Zhouyang, S.; Li, H.; Xie, Y.; Wang, Y.; Zheng, Y.; Li, Q. Nitrogen and Phosphorus Removal Coupled with Carbohydrate Production by Five Microalgae Cultures Cultivated in Biogas Slurry. *Bioresour. Technol.* **2016**, *221*, 385–393. [CrossRef]
10. Wang, L.; Chen, L.; Wu, S. Microalgae Cultivation Using Screened Liquid Dairy Manure Applying Different Folds of Dilution: Nutrient Reduction Analysis with Emphasis on Phosphorus Removal. *Appl. Biochem. Biotechnol.* **2020**, *192*, 381–391. [CrossRef]
11. Gil-Izquierdo, A.; Pedreño, M.A.; Montoro-García, S.; Tárraga-Martínez, M.; Iglesias, P.; Ferreres, F.; Barceló, D.; Núñez-Delicado, E.; Gabaldón, J.A. A Sustainable Approach by Using Microalgae to Minimize the Eutrophication Process of Mar Menor Lagoon. *Sci. Total Environ.* **2021**, *758*, 143613. [CrossRef]
12. Qin, L.; Yin, Z.; Sun, Z.; Wu, Z.; Zhu, L.; Zhou, S. Valence-Variable Iron Biostimulation: Mechanisms Insights into Enhanced Microalgae Wastewater Treatment via Transcriptomics and Proteomics. *Chem. Eng. J.* **2025**, *519*, 165577. [CrossRef]
13. Huang, H.; Zhong, S.; Wen, S.; Luo, C.; Long, T. Improving the Efficiency of Wastewater Treatment and Microalgae Production for Biofuels. *Resour. Conserv. Recycl.* **2022**, *178*, 106094. [CrossRef]

14. Le Gouic, B.; Marec, H.; Pruvost, J.; Cornet, J.F. Investigation of Growth Limitation by CO_2 Mass Transfer and Inorganic Carbon Source for the Microalga Chlorella Vulgaris in a Dedicated Photobioreactor. *Chem. Eng. Sci.* **2021**, *233*, 116388. [CrossRef]
15. Hou, Y.; Han, T.; Wu, R.; Liu, Z.; Ma, Y.; Guo, Z.; Hao, N.; Wang, W.; Ji, X.; Zhu, Z.; et al. A Novel System Integrating Electrolysis and Ionic Membranes (EIMs) Enables Artificial Carbon Concentration and Alleviation of Metal Cation Stress in Microalgae Cultivation. *Green Chem.* **2023**, *25*, 7273–7282. [CrossRef]
16. Arend, M.; Yuan, Y.; Ruiz-Sola, M.Á.; Omranian, N.; Nikoloski, Z.; Petroutsos, D. Widening the Landscape of Transcriptional Regulation of Green Algal Photoprotection. *Nat. Commun.* **2023**, *14*, 2687. [CrossRef]
17. Dao, O.; Bertrand, M.; Alseekh, S.; Veillet, F.; Auroy, P.; Nguyen, P.-C.; Légeret, B.; Epting, V.; Morin, A.; Cuiné, S.; et al. The Green Algae CO_2 Concentrating Mechanism and Photorespiration Jointly Operate during Acclimation to Low CO_2. *Nat. Commun.* **2025**, *16*, 5296. [CrossRef]
18. Singh, S.K.; Sundaram, S.; Sinha, S.; Rahman, M.A.; Kapur, S. Recent Advances in CO_2 Uptake and Fixation Mechanism of Cyanobacteria and Microalgae. *Crit. Rev. Environ. Sci. Technol.* **2016**, *46*, 1297–1323. [CrossRef]
19. Ugya, A.Y.; Sheng, Y.; Chen, H.; Wang, Q. Microalgal Bioengineering: A Futuristic Tool for Carbon Capture. *Results Eng.* **2024**, *24*, 102990. [CrossRef]
20. Hu, J.; Wang, D.; Chen, H.; Wang, Q. Advances in Genetic Engineering in Improving Photosynthesis and Microalgal Productivity. *Int. J. Mol. Sci.* **2023**, *24*, 1898. [CrossRef]
21. Li, M.-J.; Wang, R.-L.; Yang, Y.-W.; Chen, J.-X. Numerical and Experimental Analysis of Optimized Conical Flask Photobioreactor Structures to Improve Liquid–Gas Two-Phase Distribution and Microalgae Carbon Sequestration. *Appl. Therm. Eng.* **2020**, *180*, 115855. [CrossRef]
22. Cheng, J.; Xu, J.; Ye, Q.; Lai, X.; Zhang, X.; Zhou, J. Strengthening Mass Transfer of Carbon Dioxide Microbubbles Dissolver in a Horizontal Tubular Photo-Bioreactor for Improving Microalgae Growth. *Bioresour. Technol.* **2019**, *277*, 11–17. [CrossRef]
23. De Morais, M.G.; Vargas, B.P.; Da Silva Vaz, B.; Cardias, B.B.; Costa, J.A.V. Advances in the Synthesis and Applications of Nanomaterials to Increase CO_2 Biofixation in Microalgal Cultivation. *Clean. Techn Environ. Policy* **2021**, *25*, 617–632. [CrossRef]
24. Comitre, A.A.; Vaz, B.D.S.; Costa, J.A.V.; Morais, M.G.D. Renewal of Nanofibers in Chlorella Fusca Microalgae Cultivation to Increase CO_2 Fixation. *Bioresour. Technol.* **2021**, *321*, 124452. [CrossRef]
25. Yang, Y.-W.; Li, M.-J.; Hung, T.-C. Enhancing CO_2 Dissolution and Inorganic Carbon Conversion by Metal–Organic Frameworks Improves Microalgal Growth and Carbon Fixation Efficiency. *Bioresour. Technol.* **2024**, *407*, 131113. [CrossRef] [PubMed]
26. Komkhum, T.; Sema, T.; Rehman, Z.U.; In-na, P. Carbon Dioxide Removal from Triethanolamine Solution Using Living Microalgae-Loofah Biocomposites. *Sci. Rep.* **2025**, *15*, 7247. [CrossRef] [PubMed]
27. Qiu, S.; Wu, Z.; Chen, Z.; Abbew, A.-W.; Li, J.; Ge, S. Microalgal Activity and Nutrient Uptake from Wastewater Enhanced by Nanoscale Zerovalent Iron: Performance and Molecular Mechanism. *Environ. Sci. Technol.* **2022**, *56*, 585–594. [CrossRef] [PubMed]
28. Rehman, R.; Iqbal, J.; Ur Rehman, M.S.; Hamid, S.; Wang, Y.; Rasool, K.; Fazal, T. Algal-Biochar and Chlorella Vulgaris Microalgae: A Sustainable Approach for Textile Wastewater Treatment and Biodiesel Production. *Biochar* **2024**, *6*, 65. [CrossRef]
29. Wang, X.; Hou, X.; Wang, Q.; Ge, W.; Guo, S. In Situ Fabrication of Flaky-like NiMn-Layered Double Hydroxides as Efficient Catalyst for Li-O2 Battery. *J. Solid. State Electrochem.* **2019**, *23*, 1121–1128. [CrossRef]
30. Ye, H.; Liu, S.; Yu, D.; Zhou, X.; Qin, L.; Lai, C.; Qin, F.; Zhang, M.; Chen, W.; Chen, W.; et al. Regeneration Mechanism, Modification Strategy, and Environment Application of Layered Double Hydroxides: Insights Based on Memory Effect. *Coord. Chem. Rev.* **2022**, *450*, 214253. [CrossRef]
31. Mohapatra, L.; Parida, K. A Review on the Recent Progress, Challenges and Perspective of Layered Double Hydroxides as Promising Photocatalysts. *J. Mater. Chem. A* **2016**, *4*, 10744–10766. [CrossRef]
32. Budhysutanto, W.N.; Van Agterveld, D.; Schomaker, E.; Rossenaar, B.D.; Van Rosmalen, G.M.; Kramer, H.J.M. Chemical Composition and Interlayer Arrangement of Polytype 3R2 Mg–Al Layered Double Hydroxides. *Appl. Clay Sci.* **2011**, *52*, 374–380. [CrossRef]
33. Sharma, A.; Kumari, S.; Sharma, S.; Singh, T.; Kumar, S.; Thakur, A.; Bhatia, S.K.; Sharma, A.K. Layered Double Hydroxides: An Insight into the Role of Hydrotalcite-Type Anionic Clays in Energy and Environmental Applications with Current Progress and Recent Prospects. *Mater. Today Sustain.* **2023**, *22*, 100399. [CrossRef]
34. Tokudome, Y.; Fukui, M.; Iguchi, S.; Hasegawa, Y.; Teramura, K.; Tanaka, T.; Takemoto, M.; Katsura, R.; Takahashi, M. A nanoLDH Catalyst with High CO_2 Adsorption Capability for Photo-Catalytic Reduction. *J. Mater. Chem. A* **2018**, *6*, 9684–9690. [CrossRef]
35. Yang, Z.; Wei, J.; Zeng, G.; Zhang, H.; Tan, X.; Ma, C.; Li, X.; Li, Z.; Zhang, C. A Review on Strategies to LDH-Based Materials to Improve Adsorption Capacity and Photoreduction Efficiency for CO_2. *Coord. Chem. Rev.* **2019**, *386*, 154–182. [CrossRef]
36. Yong, Z.; Mata; Rodrigues, A.E. Adsorption of Carbon Dioxide onto Hydrotalcite-like Compounds (HTlcs) at High Temperatures. *Ind. Eng. Chem. Res.* **2001**, *40*, 204–209. [CrossRef]
37. Iturbe-García, J.L.; Bonifacio Martínezs, J.; Granados Correa, F.; López-Muñoz, B.E. Behavior of a Hydrotalcite Type Material Obtained from MgAl Alloy for CO_2 Adsorption. *Appl. Clay Sci.* **2019**, *183*, 105296. [CrossRef]

38. Hanif, A.; Sun, M.; Shang, S.; Tian, Y.; Yip, A.C.K.; Ok, Y.S.; Yu, I.K.M.; Tsang, D.C.W.; Gu, Q.; Shang, J. Exfoliated Ni-Al LDH 2D Nanosheets for Intermediate Temperature CO_2 Capture. *J. Hazard. Mater.* **2019**, *374*, 365–371. [CrossRef]
39. Sakr, A.A.-E.; Zaki, T.; Elgabry, O.; Ebiad, M.A.; El-Sabagh, S.M.; Emara, M.M. Enhanced CO_2 Capture from Methane-Stream Using MII -Al LDH Prepared by Microwave-Assisted Urea Hydrolysis. *Adv. Powder Technol.* **2021**, *32*, 4096–4109. [CrossRef]
40. Hadj-Abdelkader, N.E.H.; Beltrao-Nunes, A.-P.; Belkhadem, F.; Benselka, N.; Roy, R.; Azzouz, A. New Insights in MgAl and MgFe-LDH Affinity towards Carbon Dioxide—Role of the Hydrophilic Character on CO_2 Retention Strength. *Appl. Clay Sci.* **2020**, *198*, 105829. [CrossRef]
41. Hu, T.; Gu, Z.; Williams, G.R.; Strimaite, M.; Zha, J.; Zhou, Z.; Zhang, X.; Tan, C.; Liang, R. Layered Double Hydroxide-Based Nanomaterials for Biomedical Applications. *Chem. Soc. Rev.* **2022**, *51*, 6126–6176. [CrossRef]
42. Wang, L.; Ran, N.; Hu, T.; Cui, X.; Kang, Y.; Ge, M. Bioactive LDH Nanoplatforms for Cancer Therapy: Advances in Modulating Programmed Cell Death. *Mater. Today Bio* **2025**, *34*, 102139. [CrossRef]
43. Sajid, M.; Sajid Jillani, S.M.; Baig, N.; Alhooshani, K. Layered Double Hydroxide-Modified Membranes for Water Treatment: Recent Advances and Prospects. *Chemosphere* **2022**, *287*, 132140. [CrossRef] [PubMed]
44. Palmer, S.J.; Spratt, H.J.; Frost, R.L. Thermal Decomposition of Hydrotalcites with Variable Cationic Ratios. *J. Therm. Anal. Calorim.* **2009**, *95*, 123–129. [CrossRef]
45. Lund, A.; Manohara, G.V.; Song, A.-Y.; Jablonka, K.M.; Ireland, C.P.; Cheah, L.A.; Smit, B.; Garcia, S.; Reimer, J.A. Characterization of Chemisorbed Species and Active Adsorption Sites in Mg–Al Mixed Metal Oxides for High-Temperature CO_2 Capture. *Chem. Mater.* **2022**, *34*, 3893–3901. [CrossRef] [PubMed]
46. Chen, X.; Zhang, C.; Tan, L.; Wang, J. Toxicity of Co Nanoparticles on Three Species of Marine Microalgae. *Environ. Pollut.* **2018**, *236*, 454–461. [CrossRef]
47. Zamani, H. Effect of Co-Exposure of Multi-Wall Carbon Nanotubes and Cadmium on Microalga Dunaliella Salina. *J. Appl. Phycol.* **2023**, *35*, 661–671. [CrossRef]
48. Liu, T.; Wang, Y.; Li, J.; Yu, Q.; Wang, X.; Gao, D.; Wang, F.; Cai, S.; Zeng, Y. Effects from Fe, P, Ca, Mg, Zn and Cu in Steel Slag on Growth and Metabolite Accumulation of Microalgae: A Review. *Appl. Sci.* **2021**, *11*, 6589. [CrossRef]
49. Li, Y.; Xu, X.; Lei, B.; Zhuang, J.; Zhang, X.; Hu, C.; Cui, J.; Liu, Y. Magnesium-Nitrogen Co-Doped Carbon Dots Enhance Plant Growth through Multifunctional Regulation in Photosynthesis. *Chem. Eng. J.* **2021**, *422*, 130114. [CrossRef]
50. Rana, M.S.; Prajapati, S.K. Resolving the Dilemma of Iron Bioavailability to Microalgae for Commercial Sustenance. *Algal Res.* **2021**, *59*, 102458. [CrossRef]
51. Jeffers, T.L.; Purvine, S.O.; Nicora, C.D.; McCombs, R.; Upadhyaya, S.; Stroumza, A.; Whang, K.; Gallaher, S.D.; Dohnalkova, A.; Merchant, S.S.; et al. Iron Rescues Glucose-Mediated Photosynthesis Repression during Lipid Accumulation in the Green Alga Chromochloris Zofingiensis. *Nat. Commun.* **2024**, *15*, 6046. [CrossRef]
52. Zhou, H.; Wang, J.; Xu, Z.; Wang, X.; Zhang, Z.; Lan, C.Q. Two-Step Cultivation of Neochloris Oleoabundans in a Novel Horizontal Thin-Layer Algal Reactor: Interplay of pH and Dissolved Inorganic Carbon. *Biochem. Eng. J.* **2024**, *205*, 109244. [CrossRef]
53. Agbebi, T.V.; Ojo, E.O.; Watson, I.A. Towards Optimal Inorganic Carbon Delivery to Microalgae Culture. *Algal Res.* **2022**, *67*, 102841. [CrossRef]
54. Sade, Z.; Hegyi, S.; Halevy, I. Equilibration Times of Dissolved Inorganic Carbon During pH Transitions. *Front. Earth Sci.* **2022**, *9*, 792858. [CrossRef]
55. Wu, Q.; Li, S.; Wang, H.; Wang, W.; Gao, X.; Guan, X.; Zhang, Z.; Teng, Y.; Zhu, L. Construction of an Efficient Microalgal-Fungal Co-Cultivation System for Swine Wastewater Treatment: Nutrients Removal and Extracellular Polymeric Substances (EPS)-Mediated Aggregated Structure Formation. *Chem. Eng. J.* **2023**, *476*, 146690. [CrossRef]
56. Xiao, R.; Zheng, Y. Overview of Microalgal Extracellular Polymeric Substances (EPS) and Their Applications. *Biotechnol. Adv.* **2016**, *34*, 1225–1244. [CrossRef] [PubMed]
57. Sun, X.-M.; Ren, L.-J.; Ji, X.-J.; Huang, H. Enhancing Biomass and Lipid Accumulation in the Microalgae *Schizochytrium* sp. by Addition of Fulvic Acid and EDTA. *AMB Expr.* **2018**, *8*, 150. [CrossRef]
58. Shi, W.; Zhang, G.; Li, F.; Feng, J.; Chen, X. Two-Step Adsorption Model for Pb Ion Accumulation at the Algae-Water Interface in the Presence of Fulvic Acid. *Sci. Total Environ.* **2020**, *742*, 140606. [CrossRef]
59. Liu, X.; Ji, B.; Li, A. Enhancing Biolipid Production and Self-Flocculation of Chlorella Vulgaris by Extracellular Polymeric Substances from Granular Sludge with CO_2 Addition: Microscopic Mechanism of Microalgae-Bacteria Symbiosis. *Water Res.* **2023**, *236*, 119960. [CrossRef] [PubMed]
60. Hao, T.-B.; Zhang, Z.-H.; Hu, L.-L.; Liu, S.-F.; Mou, J.-H.; Yang, P.; Yuan, Z.; Zhang, Q.; Balamurugan, S.; Yang, W.-D.; et al. Dissolved Organic Matter-Mediated Metabolic Shifts in Chlorella Sorokiniana Enhanced Bioremediation of Multi-Ionic Stress. *J. Hazard. Mater.* **2025**, *496*, 139350. [CrossRef] [PubMed]
61. Xia, Z.; Ng, H.Y.; Bae, S. Synergistic Microalgal-Bacterial Interactions Enhance Nitrogen Removal in Membrane-Aerated Biofilm Photoreactors Treating Aquaculture Wastewater under Salt Stress: Insights from Metagenomic Analysis. *Water Res.* **2025**, *283*, 123878. [CrossRef]

62. Chen, W.; Westerhoff, P.; Leenheer, J.A.; Booksh, K. Fluorescence Excitation−Emission Matrix Regional Integration to Quantify Spectra for Dissolved Organic Matter. *Environ. Sci. Technol.* **2003**, *37*, 5701–5710. [CrossRef]
63. Strotmann, U.J.; Eismann, F.; Hauth, B.; Bias, W.R. An Integrated Test Strategy for the Assessment of Anaerobic Biodegradability of Wastewaters. *Chemosphere* **1993**, *26*, 2241–2254. [CrossRef]

Disclaimer/Publisher's Note: The statements, opinions and data contained in all publications are solely those of the individual author(s) and contributor(s) and not of MDPI and/or the editor(s). MDPI and/or the editor(s) disclaim responsibility for any injury to people or property resulting from any ideas, methods, instructions or products referred to in the content.